ceramics

MDPI

Article

Hybrid Atmosphere Processing of Lead-Free Piezoelectric Sodium Potassium Niobate-Based Ceramics

Astri Bjørnetun Haugen

Department of Energy Conversion and Storage, Technical University of Denmark, Frederiksborgvej 399, 4000 Roskilde, Denmark; ahua@dtu.dk

Received: 20 May 2019; Accepted: 5 July 2019; Published: 17 July 2019

Abstract: $K_{0.5}Na_{0.5}NbO_3$-based ceramics, a promising group of lead-free piezoelectrics, are challenging to sinter dense while avoiding alkali evaporation. This work explores hybrid atmosphere processing, a new approach where reducing atmospheres is used during heating to avoid coarsening from alkali carbonates and hydroxides, and oxidizing atmospheres is used during sintering to avoid alkali evaporation. Discs of $Li_{0.06}(K_{0.52}Na_{0.48})_{0.94}Nb_{0.71}Ta_{0.29}O_3$ with 0.25 mol% Mn (KNNLTM) were sintered in air, N_2, 9% H_2 in N_2, or 9% H_2 in N_2 during heating and air during sintering (hybrid atmosphere processing). The highest density was obtained by sintering in 9% H_2 in N_2, but resulted in high alkali loss and decomposition of the surface, followed by low piezoelectric response. However, with the hybrid H_2/air processing it was possible to both avoid surface decomposition and leakage currently associated with alkali evaporation during sintering in H_2, and to obtain a denser, more phase-pure and small-grained KNNLTM ceramic with a higher piezoelectric response than obtained by sintering in air or N_2.

Keywords: piezoelectrics; ferroelectrics; lead-free ceramics; sintering; microstructure

1. Introduction

$K_{0.5}Na_{0.5}NbO_3$ (KNN) is one of the most promising lead-free alternatives to traditional, lead-based piezoceramics [1]. KNN is often doped with ~5–7% Li and ~10–20% Ta, which lower its orthorhombic-tetragonal polymorphic phase transition to close to room temperature and increases the (room temperature) piezoelectric response [2–4]. Mn is often added to reduce the leakage current and improve sintering [5,6]. Recently, Huo, et al. [7] presented a [100]-oriented single crystal of $Li_{0.06}(K_{0.52}Na_{0.48})_{0.94}Nb_{0.71}Ta_{0.29}O_3$ with 0.25 mol% Mn (KNNLTM) with very high piezoelectric coefficients, including a k_{33} of 0.95. This record-high k_{33} is very promising for applications in ultrasound transducers [8]. Yet, since single crystals are expensive and limited in size, it is interesting to study this specific KNN-based composition also as a ceramic, and eventually a textured [2,9–12] material.

Sintering of KNN-based ceramics is, however, challenging [13]. This has several causes: The temperature window for densification is narrow, the alkali elements are volatile, and the particles and grains are prone to coarsen rather than to densify. The optimal sintering temperature is reported around 1100 °C for pure KNN, and usually a little higher for Li, Ta-doped KNN [14,15], which is close to the solidus temperature (1140 °C in pure KNN [16]). The increasing volatility of the alkali elements with temperature must also be considered, since their evaporation is noticeable already at 1000 °C [17]. The risk of evaporation should also be kept in mind when choosing the sintering dwell time, which is a trade-off between complete densification (and templated grain growth in the case of textured ceramics [9]) and loss of the volatile alkali elements. The affected surfaces can be machined off in the case of bulk ceramics, but for thick or thin films or complex geometries such as fibers or

3D-printed structures, this is not a viable approach. Careful control of the sintering conditions is therefore critical, and the optimal conditions should be investigated carefully for each composition and type of starting powder.

Reducing atmospheres have been investigated in recent years for sintering of KNN-based ceramics [18–23]. The reducing atmosphere enables co-firing with inexpensive base metal electrodes [23], and is also shown in some studies to improve densification without lowering dielectric and piezoelectric response [22]. The increased densification has been attributed to a change from faceted to rough grain boundaries when more oxygen vacancies are introduced, which suppresses abnormal grain growth [18]. Changes in the microstructure might directly impact the piezoelectric response [24,25], and at the same time, the reducing atmospheres increases the extent of evaporation of alkali oxide species [26]. Reducing the metal ions is also a risk, and annealing in oxidizing atmospheres after sintering might, therefore, be necessary [27].

In addition to abnormal grain growth at high temperatures, abnormal growth and coarsening of KNN-based powders can also be a problem at lower temperatures, hindering further densification [26,28,29]. The reactivity of the alkali elements towards ambient CO_2 and H_2O can be a cause of this coarsening: Alkali carbonates or hydroxides have low melting points and can form a transient liquid phase at low temperatures (~800 °C) that promotes particle coarsening [26]. This is especially pronounced in alkali-excess KNN [26,29], but expected to occur to some extent also in stoichiometric KNN. The hygroscopicity of alkali carbonate precursors for solid-state synthesis of KNN is well known and accounted for by drying raw materials before weighing [13], but reactivity during the heating step towards sintering is neglected.

A novel approach explored in this work is therefore hybrid atmosphere processing. This entails reducing atmosphere during the heating step (to decompose any alkali carbonates or hydroxides and thus avoid transient liquid phases causing coarsening), and oxidizing atmosphere during sintering (to avoid excessive alkali evaporation). The motivation of this work is hence to investigate the hybrid atmosphere processing for improved densification and piezoelectric response, with the specific KNNLTM composition as the test system, such that we can study this promising composition also as a ceramic. The results show that KNNLTM piezoelectric ceramics with 91% density and a d_{33} of 130 pC/N can be made using the hybrid atmosphere processing, and that this condition provides the optimum combination of phase purity, density and piezoelectric response.

2. Materials and Methods

KNNLTM powder made by spray pyrolysis and calcined at 600 °C was purchased from Cerpotech A/S, Tiller, Norway. Its surface area was measured by the Brunauer–Emmett–Teller (BET) method with N_2 (Quantachrome Autosorp 1 MP, Anton Paar, Ostfildern, Germany). Dilatometry studies were performed with a 2 °C/min heating rate in air (DIL 402, Netzsch, Selb, Germany). The pH of distilled water with KNNLTM powder dispersed in it (~10 wt% powder) was measured with universal pH indicator strips. A small amount of the as-received powder was calcined again at 800 °C for 6 h to study the grain growth.

Samples for sintering were prepared by uniaxially pressing powder into 12 mm diameter discs of ~2–3 mm height with pressing tools lubricated with stearic acid. The discs were sintered on an alumina substrate with some coarse KNNLTM powder as a sintering bed, inside a tube furnace with flowing gas (60 mL/min). Sintering was performed in the temperature range 1000–1125 °C with a 2–20 h dwell time. Heating and cooling rates were 200 °C/h. The gas was varied between air, N_2, 9% H_2 in N_2 (hereafter denoted in brevity as H_2) and the hybrid atmosphere processing. The latter means a split between 9% H_2 in N_2 and air (hereafter denoted as H_2/air), where the heating up to 800 °C was performed in H_2, before the tube was flushed with N_2 for 10 min and the gas changed to air for the remaining heating ramp, sintering and cooling. Some H_2-sintered samples were annealed after sintering to reduce their leakage current. The annealing was performed at 650 °C for 4 h in a large chamber furnace with stagnant, ambient air. X-ray diffraction (XRD) patterns were recorded from

the as-sintered top surface with a Bruker D8 (Bruker, Billerica, MA, USA). Density was measured by the Archimedes method in isopropanol. Scanning electron microscopy (SEM) images were recorded with backscatter mode using a Merlin (Zeiss, Berlin, Germany) or TM3000 (Hitachi, Tokyo, Japan). Energy-dispersive spectroscopy (EDS) was performed with model SDD (Bruker, Billerica, MA, USA), the reported data was averages taken from three whole-area scans. Both SEM and EDS were performed on surface of the as-sintered sample surface. Grain sizes were measured from these images (with an average of ~100 grains) using the software Image J.

Samples were electroded with Ag paste (LVOC, SPI, West Chester, PA, USA) prior to electrical characterization. Ferroelectric hysteresis loops were measured with a piezoelectric evaluation system (aixPES, aixACCT, Aachen, Germany). The piezoelectric charge coefficient (d_{33}) was measured after >24 h with a d_{33}-m (APC International Ltd., Mackeyville, PA, USA).

3. Results

3.1. Powder Properties of KNNLTM

The X-ray diffractogram of the as-received KNNLTM powder is shown in Figure 1. The peaks were wide and no peak splitting was therefore visible, but all main reflections can be assigned to a perovskite structure similar to that of $KNbO_3$ (PDF 32-0822). There were two low-intensity reflections at 20° and 30° 2θ that did not belong to the perovskite phase, but matched with K_3NbO_4 (PDF 52-1894). The dilatometry curve of the as-received KNNLTM powder (Figure 2) showed that the powder started densifying at very low temperatures. At ~700 °C there was a sudden decrease in the dimensions of the pellet, indicative of a rapid rearrangement of the powder, typically in the presence of a liquid phase. This shrinkage stopped already at ~800 °C, where the sample started to slightly expand. This indicated that the rapid rearrangement had been completed, and due to the lack of shrinkage we can see the thermal expansion. After reaching ~950 °C the sample started shrinking slowly again, which means a densifying sintering mechanism (lattice or grain boundary diffusion) had been thermally activated. The shrinkage continued at a slow rate until it accelerated again around 1125 °C, possibly related to a partly melting of the sample. The dilatometry was only performed up to 1150 °C to avoid the risk of the sample melting in the dilatometer, such that we cannot observe when the shrinkage flattened out in this final stage of the sintering. This is common for KNN-based ceramics due to their narrow densification window close to the liquidus temperature [13].

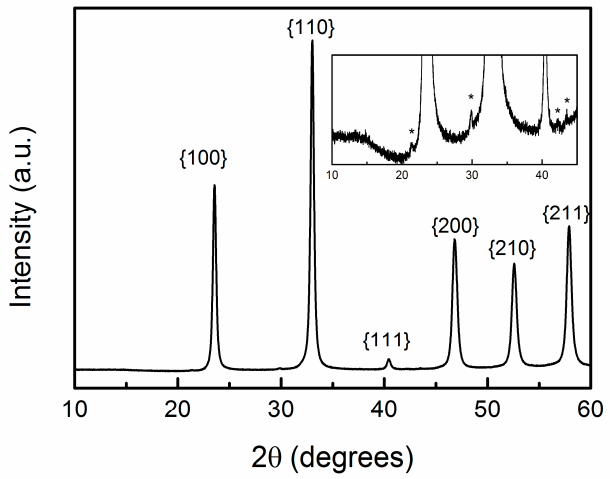

Figure 1. XRD of $Li_{0.06}(K_{0.52}Na_{0.48})_{0.94}Nb_{0.71}Ta_{0.29}O_3$ with 0.25 mol% Mn (KNNLTM) powder with reflections indexed to the $KNbO_3$-like perovskite structure (PDF 32-0822). The inset shows a close-up of the low-intensity region where reflections from additional phases are marked with *.

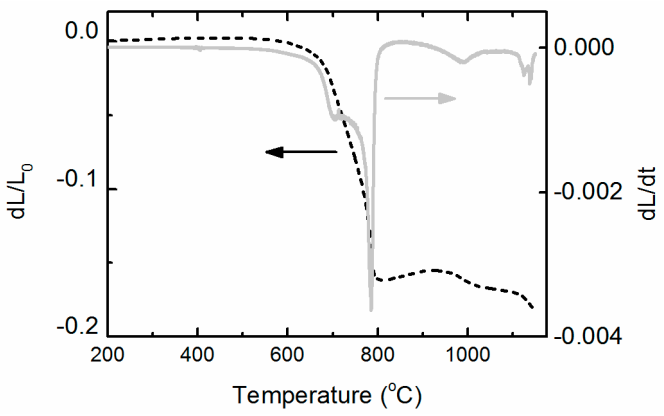

Figure 2. Shrinkage and shrinkage rate of KNNLTM powder in air.

Micrographs of the as-received powder and the powder calcined at 800 °C are shown in Figure 3. Here, we can see that the as-received powder (Figure 3a) consisted of fine particles of size well below ~300 nm and some larger (up to ~500 nm) agglomerates of these particles that remained from the spheres of dried precursor droplets formed during spray pyrolysis. A primary particle size of 53 nm was calculated from the specific surface area of 22.5 m^2/g measured by BET. After heat treating the powder at 800 °C in air, the particles coarsened to 0.5–1 µm and the grains had a cuboidal shape (Figure 3b), while if this heat treatment was performed in H_2 instead (Figure 3c), the particle size remained similar as the as-received powder. A dispersion of the as-received KNNLTM powder in distilled water had a pH of 9–10.

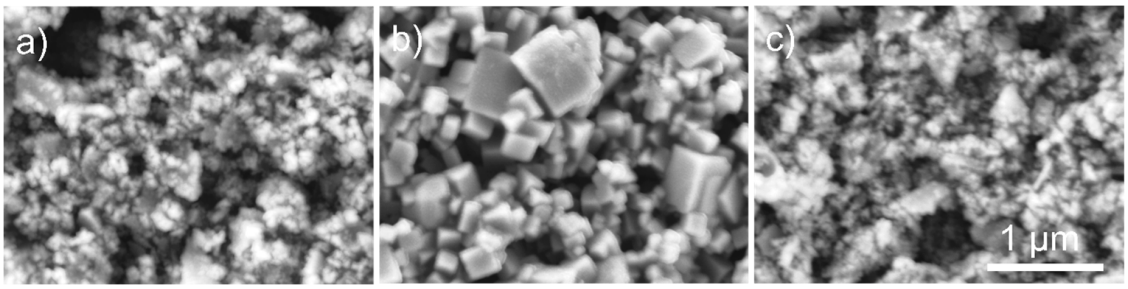

Figure 3. SEM images of KNNLTM powder; (**a**) as received, (**b**) after calcination at 800 °C in air and (**c**), after calcination at 800 °C in H_2.

3.2. Sintering of KNNLTM

The effect of sintering atmosphere and temperature on the density after sintering is shown in Figure 4a. The largest density at all sintering temperatures were observed with H_2, where above 95% of the theoretical density was reached. This density was significantly higher than for the other sintering atmospheres, the closest was the hybrid processing in H_2/air where ~90% density was reached. Samples sintered in N_2 vs. air were very similar, both atmospheres resulted in densities up to 88%. Figure 4b shows that the sintering conditions also markedly affect the weight loss during sintering. For all atmospheres, there was an increase in the weight loss with sintering temperature, and especially above 1075 °C. Some weight loss (in the order of 1%) was expected due to the stearic acid pressing tool lubricant, but at all temperatures, the H_2-sintered samples had a significantly higher weight loss (~3–4 wt%), that was also higher than the other samples (~1.5–2.5 wt%). Longer dwell times also increased the density (Figure 5a), 97% density was achieved in H_2 at 1075 °C by increasing the sintering time to 14 h, but accompanied by a further increase in the weight loss (up to 4.5 wt%) (Figure 5b). Samples sintered in H_2 were dark blue, almost black, with the top, as-sintered surface a little darker

than the polished surface. The blue color was previously reported in reduced KNN and assumed to originate from a reduction of Nb^{5+} to Nb^{4+} [30]. Upon annealing in air at 650 °C, these samples changed color from blue to beige, also as previously observed [31,32]. All the other samples were pink/beige after sintering.

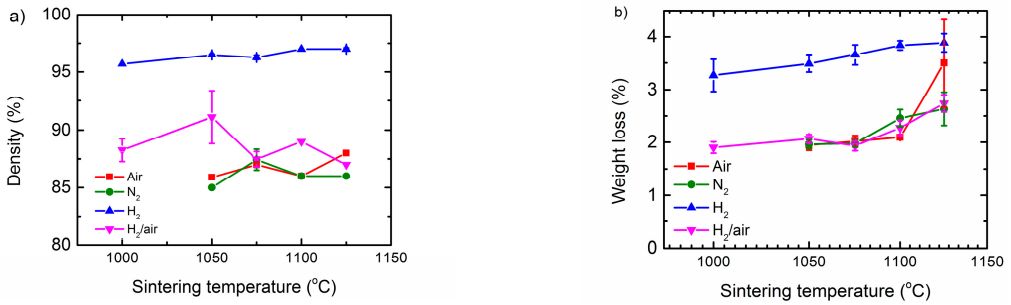

Figure 4. (**a**) Density and (**b**) weight loss of KNNLTM ceramics vs. sintering temperature in various atmospheres. The sintering dwell time was 2 h.

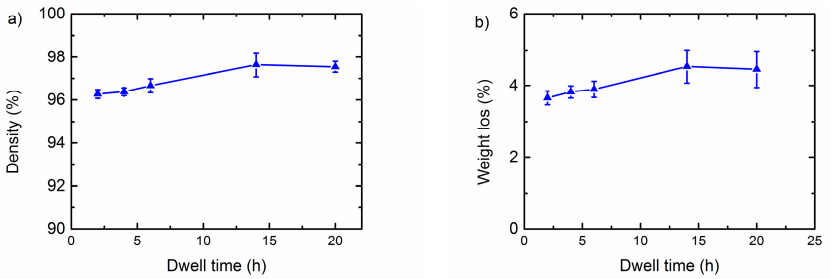

Figure 5. (**a**) Density and (**b**) weight loss of KNNLTM ceramics vs. sintering dwell time at 1075 °C in H_2.

3.3. Phase and Microstructure of the Sintered KNNLTM

XRD patterns in Figure 6 show how the sintering conditions affected the phase composition of the KNNLTM samples. The main phase in all samples sintered at 1100 °C can be assigned to a perovskite structure similar to that of $KNbO_3$ (PDF 32-0822). All diffractograms also contained some additional reflections (e.g., at ~26° and 29–30° 2θ). The secondary phase amount was right above the XRD detection limit after sintering in all atmospheres, except H_2 where the top surface had a significant amount of these secondary phases. This decomposition of the top surface was strongly temperature dependent. Figure 7 shows how the amount of secondary phase increased drastically with temperature between 1050 and 1075 °C. Also, this large content of secondary phase was a surface phenomenon, after polishing off the outer ~100 μm, the sample appeared as a phase-pure KNNLTM.

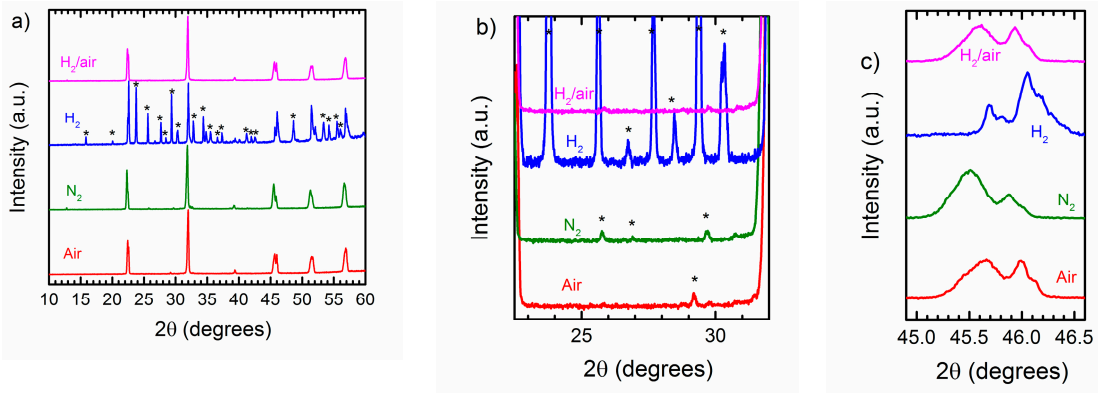

Figure 6. (**a**) XRD patterns of as-sintered surface of KNNLTM after sintering for 2 h in various atmospheres at 1100 °C. Asterisks (*) indicate reflections not assigned to the KNNLTM phase (according to $KNbO_3$, PDF 32-0822). (**b**) and (**c**) are close-ups of different regions of (**a**).

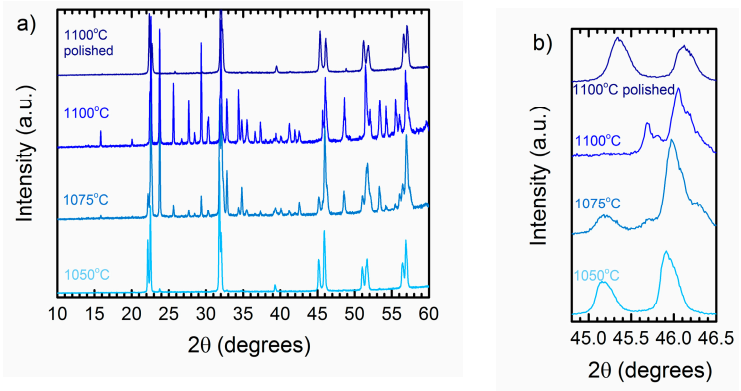

Figure 7. (**a**) XRD patterns of KNNLTM ceramics sintered in H_2, and the effect of polishing off the surface. (**b**) Close-up from (**a**).

The sintering atmosphere also affected the structure of the KNNLTM main phase. From the close-up of the $(200)_{pc}$ reflections in Figure 6c, we can see from the distance and ratio between the lower and higher 2θ reflections) that the KNNLTM appeared tetragonal (*P*4*mm*) after sintering in H_2, while otherwise predominantly orthorhombic (*Amm*2) or a mixture of both phases. The reflections of the H_2-sintered samples also shifted to higher 2θ values, more at higher temperatures (Figure 7b) indicating a smaller unit cell. Both a decrease in cell volume and increase in tetragonal relative to orthorhombic phase after reducing conditions is in accordance with previous observations [13,33]. The similarity in the peak shape and position between H_2/air and air (Figure 6c) in this study also shows that the high-temperature atmosphere (as opposed to the low-temperature atmosphere) has the largest influence on the structure of the KNNLTM composition.

The sintering atmosphere also largely impacts the microstructure, as can be seen from the SEM images in Figure 8. All samples except the H_2-sintered feature the cuboid grains typical of KNN-based ceramics. The hybrid atmosphere processed H_2/air samples, however, also contained a large fraction of smaller, rounder grains. The grain size (Table 1) varied significantly with the sintering atmosphere, the grains were finer after sintering in H_2 and H_2/air (~1.5 µm) than air and N_2 (~3.5 µm). After sintering in H_2, the surface was completely decomposed: Individual grains were not easily distinguishable and the surface resembled a frozen liquid phase with some cracks. The samples sintered in air and N_2 also contained large amounts of a secondary phase. This phase was darker, and less defined in shape than the KNNLTM grains. It is not observable in the samples sintered in H_2 and H_2/air.

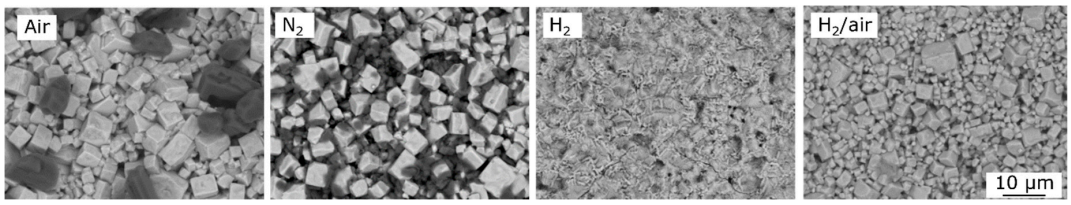

Figure 8. SEM images (backscatter mode) of KNNLTM after sintering for 2 h at 1100 °C in various atmospheres.

Table 1. Grain size of KNNLTM ceramics after sintering for 2 h at 1100 °C in various atmospheres.

	Air	**N_2**	**H_2**	**H_2/Air**
Grain size (µm)	3.36 ± 1.43	3.64 ± 1.54	N/A	1.46 ± 0.67

The results from EDS analysis are shown in Figure 9. The nominal amounts (calculated without Li, which is undetectable by EDS) are indicated with dotted lines. After sintering in air at 1100 °C for 2 h, the composition was close to the nominal, but with slightly smaller amounts of Nb and Ta, corresponding to an A/B site elemental ratio of 1.30 (above 1 = alkali excess). Elemental ratios corresponding to alkali excess were also seen after sintering in N_2 (2.12) and to a small extent in H_2/air (1.15). The largest change in chemical composition was, however, observed after sintering in H_2. Here, both of the alkali elements were significantly reduced in quantity (and the relative amounts of Nb and O increased, correspondingly), such that the A/B ratio now was 0.17 (below 1 = alkali deficient). The EDS analysis should be considered as a qualitative guide more than an accurate quantification due to inaccuracies in detecting and quantifying elements on a slightly rough surface. Still, we can use the elemental maps (Figure 9b) to learn about the secondary phases. In N_2, there is a large amount of K, concentrated in the dark secondary phase between the KNNLTM grains. The dark secondary phase was also enriched in K in the air-sintered samples. Ta was distributed similarly as Nb after sintering in either N_2 or air: Homogenous within the KNNLTM grains and mainly absent in the secondary phase.

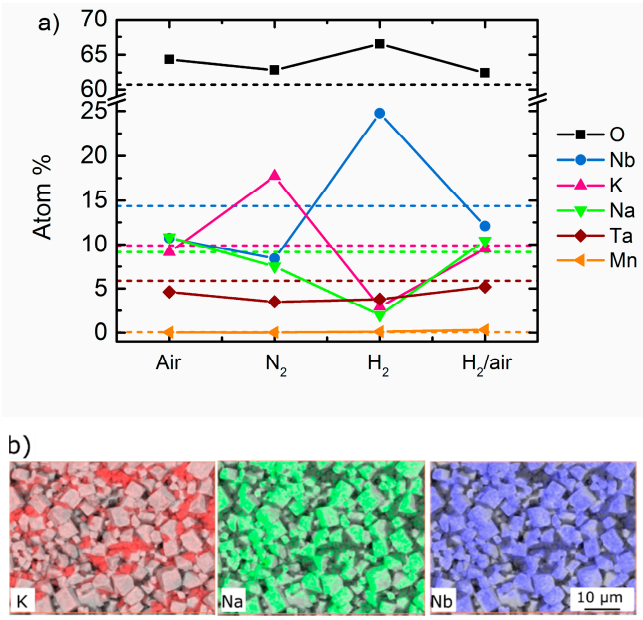

Figure 9. (**a**) Elemental composition in KNNLTM as observed by energy-dispersive spectroscopy (EDS) after sintering at 1100 °C (the solid lines are guides for the eyes and the dotted lines represent the nominal composition). (**b**) Map of K, Na and Nb distribution after sintering in N_2.

3.4. Piezo- and Ferro-electric Response of KNNLTM Ceramics

The hysteresis loops after sintering, and sintering and annealing are shown in Figure 10a. The sample sintered in H_2 was too conductive to hold an electric field prior to annealing, and a hysteresis loop could not be recorded. The other samples show a well-developed hysteresis loop with remnant polarization (P_r) of ~15 μC/cm^2 and a coercive field (E_c) of ~1.5 kV/mm. The hysteresis loop of the H_2-sintered and annealed KNNLTM showed similar P_r as for the other sintering conditions, but has a stronger contribution from leakage currents, observed as the unclosed, wider and less defined hysteresis curves and apparent higher E_c. The piezoelectric charge coefficient (d_{33}) is shown in Figure 10b. The samples sintered in H_2 showed very weak piezoelectric response, also after annealing, with a maximum d_{33} of 30 pC/N. The highest response was found after the hybrid atmosphere processing with H_2/air, here the d_{33} reached 130 pC/N.

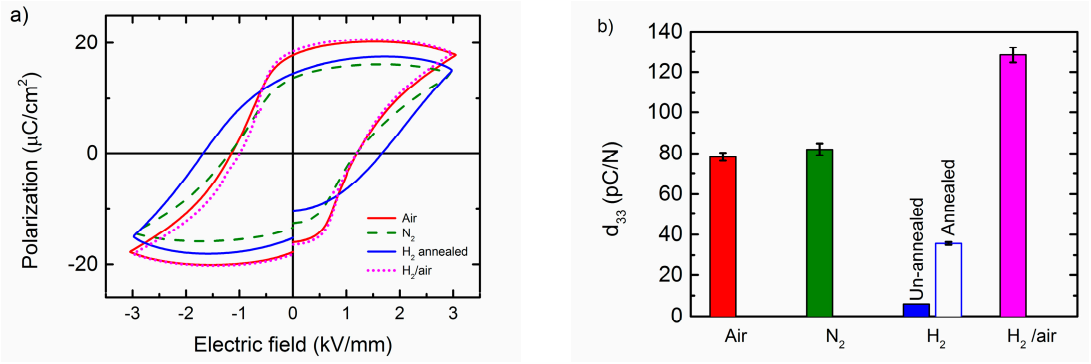

Figure 10. (**a**) Polarization vs. electric field of KNNLTM sintered for 2 h at 1100 °C in various atmospheres (un-annealed H_2-sintered samples are not shown since they were too conductive to hold a field) and (**b**), their piezoelectric coefficient d_{33}.

4. Discussion

4.1. KNNLTM Powder and Coarsening

The powder characterization reveals the KNNLTM powder to be very fine. The small powder size (as seen by SEM, BET and the wide peaks of the XRD pattern) should intuitively be beneficial for sintering. However, we also know that the large surface area increases the reactivity towards atmospheric CO_2 and H_2O and formation of alkali hydroxides and carbonates, for example [34,35]:

$$K_2O\ (s) + CO_2\ (g) = K_2CO_3\ (l, s) \quad (1)$$

$$K_2O\ (s) + H_2O\ (g) = 2\ KOH\ (l, s) \quad (2)$$

This has previously been shown to cause coarsening into cuboid particles at low temperatures (~800 °C) and limit further densification, especially with alkali-excess powder [26,29]. Signs of alkali excess [26] are also observed in this work: The high pH of powder in water, the large particle size after an extra calcination at 800 °C in air, the rapid densification at low temperatures followed by limited further densification at higher temperatures, and an A/B element ratio above 1 after sintering in air. Reducing conditions decompose alkali species such as hydroxide or carbonates and limits particle coarsening during heating, as directly observed in Figure 3 in this work.

4.2. Densification and Microstructure of KNNLTM Ceramics

The smaller and rounder grains within KNNLTM ceramics exposed to reducing conditions (H_2 and H_2/air) is in agreement with previous results [36]. In general, the KNNLTM grain size is relatively small after sintering compared to other KNN-based ceramics from solid state synthesis [13,29],

probably a benefit of the fine starting particle size from the spray pyrolysis-made [26] powder. The high densification after sintering in H_2 relative to the other atmospheres is also in accordance with previously work [36], where it has been attributed to change from faceted to rough grain boundaries. This work demonstrates high density in H_2-sintered samples because the reducing atmosphere avoids coarsening by removing the adsorbed carbonate and hydroxide species during the heating stage. Since the density is higher than after the H_2/air hybrid processing (where we also avoid this low-temperature coarsening) the densification may also have been assisted by a liquid phase formed during sintering by melting an alkali deficient, lower liquidus temperature secondary phase (see also discussion on surface decomposition in Section 4.3).

4.3. Chemical Stability of Sintered KNNLTM Ceramics

Optimal sintering conditions of KNN should not be considered only in terms of densification, but also alkali evaporation. In both Figures 4 and 5, the increase in density after sintering in H_2 or with increasing dwell time appears to be directly correlated with the weight loss. As the alkali elements are more volatile than the other elements in KNNLTM [37], deviations from the nominal stoichiometry is expected after sintering. The EDS study (Figure 9) clearly demonstrates an overall slight alkali excess on the surface after sintering in air. However, the content of K and Na decrease relative to Nb in reducing conditions, where their evaporation rate is known to be higher [26]. After sintering in H_2/air, the stoichiometry is close to the nominal, demonstrating the hybrid atmosphere processing with H_2 only during heating to be suitable for high densification relative to air or N_2, while at the same time avoiding weight loss and stoichiometry changes.

Since the secondary phase observed by backscatter SEM in air- and N_2-sintered KNNLTM is darker than the KNNLTM phase, it must have a lower average atomic number. This secondary phase is therefore either alkali-rich, or a hydrated version of an alkali-deficient phase. Since it is not visible after sintering in H_2 and H_2/air, these conditions either remove any alkali-rich phases present in the powder, or remove the H_2O and/or CO_2 required to form hydrated secondary phases. However, Figure 9b clearly show that the secondary phases are enriched in K and depleted of Nb relative to the bulk phase, and the secondary phase must therefore be alkali excess. Alkali carbonates and hydroxides are amorphous, which explains why we cannot observe them in the XRD diffractograms of these samples.

Secondary phases are usually present to some extent in KNN-based ceramics after sintering, typically Nb-rich tungsten-bronze structured phases (e.g., $K_4Nb_6O_{17}$ (PDF 76-0977) and/or $K_{5.75}Nb_{10.85}O_{30}$ (PDF 38-0297)) or their hydrated versions [29]. It is also often observed that more than 7–8% $LiTaO_3$ doping in KNN causes formation of $K_3Li_2Nb_5O_{15}$ (PDF 52-0157) [38]. In this work, such alkali-deficient secondary phase similar to $K_4Nb_6O_{17}$ and $K_{5.75}Nb_{10.85}O_{30}$ can only definitely be found on the surface of the H_2-sintered samples (not to be confused with the dark, amorphous secondary phase visible by SEM after sintering in air and N_2). The top surface of these samples after sintering at ≥1075 °C in H_2 decomposed and resembled a frozen liquid phase, slightly cracked during cooling due to thermal expansion differences. This phenomenon can be explained by the lower liquidus temperature of the phases on the alkali-deficient side of the $KNbO_3$ phase diagram [39]. Alkali evaporation makes this phase form on the surface in reducing conditions, and the surface therefore partly melts during sintering and freezes again during cooling.

4.4. Piezo- and Ferro-electric Response of KNNLTM Ceramics

Hybrid atmosphere processing, with reducing conductions during heating and oxidizing during sintering gives the KNNLTM ceramics with the highest piezoelectric response. This can be attributed to higher density, closer to stoichiometric composition, and smaller grains relative to the other compositions. The ferro- and piezo-electric response of all samples are as expected relative to the [100]-oriented single crystal of the same composition by Huo, et al. [7]. In the ceramics the P_r is higher (expected since the single crystal is not oriented parallel to its polar axis [40]), the E_c is larger, and the piezoelectric coefficient is lower. All values of the ceramics are, however, in the same range as typically

reported for KNN-based ceramics [15], with exception of the leaky, H_2-sintered samples. Leakage current can be lowered in KNN (and other ferroelectrics) through doping with Mn, due to its mixed valence state (2+, 3+, 4+) and ability to absorb free charge carriers, e.g.,

$$Mn^{2+} + h^{+} = Mn^{3+} \quad (3)$$

$$Mn^{4+} + e^{-} = Mn^{3+} \quad (4)$$

In reducing conditions, n-type conductivity is expected due to formation of oxygen vacancies and reduction of Nb^{5+} to Nb^{4+} with an conductive 4*d* electron [41]. At the same time, the reducing conditions will transform all manganese to Mn^{2+} [33], such that leakage current mediation through Equation (4) is not possible. Mn doping might therefore expand the pO_2 region where the sample has low leakage [30,42], but is not sufficient to prevent leakage current when sintering in H_2. The leakage current of the H_2-sintered samples decreased upon annealing in air, confirming the n-type conductivity in reduced samples. All KNNLTM ceramics in this work show signs of some leakage current (rounded, unclosed hysteresis curves), probably related to alkali-excess secondary phases and their possible hydration [29,43].

5. Conclusions

Hybrid atmosphere processing, where a reducing atmosphere is used during heating and an oxidizing during sintering, was tested on the lead-free piezoelectric $Li_{0.06}(K_{0.52}Na_{0.48})_{0.94}Nb_{0.71}Ta_{0.29}O_3$ (KNNLTM). An atmosphere of 9% H_2 in N_2 was used during heating up to 800 °C to remove alkali carbonates and hydroxides in the powder, before switching to air for the remaining part of the sintering to limit alkali evaporation. With this approach, it was possible to remove alkali-containing adsorbed species and with this the low-temperature coarsening of the powder. The hybrid processing therefore resulted in higher density and piezoelectric response than after sintering in N_2 or air, and without compromising the KNNTLM phase stability. The highest density was found after sintering in 9% H_2 in N_2, but was accompanied by high weight loss, alkali evaporation and decomposition of the KNNLTM phase on the surface. Although the large amounts of secondary phase can be avoided by lowering the sintering temperature or polishing off the surface, the piezoelectric response is low, and only present after an extra annealing step. Sintering in H_2 is therefore not a suitable approach for KNNLTM, and should only be considered if co-sintering with base-metal electrodes is required. The hybrid atmosphere processing approach on the other hand, might find use for sintering of any KNN-based piezoelectrics, or even be used to improve the sintering of other alkali oxide ceramics.

Funding: This research was funded by Independent Research Fund Denmark, grant DFF-6111-00440, Siemensfonden and Brødrene Hartmanns Fond.

Acknowledgments: The author would like to thank Paul Douaneau, Moises Espindola Rodriguez, Jette Iversen and Pernille Hedemark Nielsen for assistance with sample fabrication and characterization.

Conflicts of Interest: The author declares no conflict of interest. The funders had no role in the design of the study; in the collection, analyses, or interpretation of data; in the writing of the manuscript, or in the decision to publish the results.

References

1. Rödel, J.; Jo, W.; Seifert, K.T.P.; Anton, E.M.; Granzow, T.; Damjanovic, D. Perspective on the development of lead-free piezoceramics. *J. Am. Ceram. Soc.* **2009**, *92*, 1153–1177. [CrossRef]
2. Saito, Y.; Takao, H.; Tani, T.; Nonoyama, T.; Takatori, K.; Homma, T.; Nagaya, T.; Nakamura, M. Lead-free piezoceramics. *Nature* **2004**, *432*, 84. [CrossRef] [PubMed]
3. Wang, X.; Wu, J.; Xiao, D.; Zhu, J.; Cheng, X.; Zheng, T.; Zhang, B.; Lou, X.; Wang, X. Giant Piezoelectricity in Potassium—Sodium Niobate Lead-Free Ceramics. *J. Am. Chem. Soc.* **2014**, *5*, 3–8. [CrossRef] [PubMed]
4. Hollenstein, E.; Davis, M.; Damjanovic, D.; Setter, N. Piezoelectric properties of Li- and Ta-modified $(K_{0.5}Na_{0.5})NbO_3$ ceramics. *Appl. Phys. Lett.* **2005**, *87*, 182905. [CrossRef]

5. Lin, D.; Kwok, K.W.; Tian, H.; Chan, H.W.L. Phase transitions and electrical properties of $(Na_1$-xKx)$(Nb_1$-ySby) O_3 lead-free piezoelectric ceramics with a MnO_2 sintering aid. *J. Am. Ceram. Soc.* **2007**, *90*, 1458–1462. [CrossRef]
6. Abazari, M.; Safari, A.; Akdogan, E.K. Effect of manganese doping on remnant polarization and leakage current in (K 0.44, Na 0.52, Li 0.04) (Nb 0.84, Ta 0.10, Sb 0.06) O3 epitaxial thin films on Sr TiO_3. *Appl. Phys. Lett.* **2008**, *92*, 212903. [CrossRef]
7. Huo, X.; Zhang, R.; Zheng, L.; Zhang, S.; Wang, R.; Wang, J.; Sang, S.; Yang, B.; Cao, W. (K, Na, Li)(Nb, Ta)O3:Mn Lead-Free Single Crystal with High Piezoelectric Properties. *J. Am. Ceram. Soc.* **2015**, *98*, 1829–1835. [CrossRef] [PubMed]
8. Shung, K.K.; Cannata, J.M.; Zhou, Q.F. Piezoelectric materials for high frequency medical imaging applications: A review. *J. Electroceram.* **2007**, *19*, 139–145. [CrossRef]
9. Messing, G.L.; Trolier-McKinstry, S.; Sabolsky, E.M.; Duran, C.; Kwon, S.; Brahmaroutu, B.; Park, P.; Yilmaz, H.; Rehrig, P.; Eitel, K.; et al. Templated Grain Growth of Textured Piezoelectric Ceramics. *Key Eng. Mater.* **2004**, *29*, 45–96. [CrossRef]
10. Messing, G.L.; Poterala, S.; Chang, Y.; Frueh, T.; Kupp, E.R.; Watson, B.H.; Walton, R.L.; Brova, M.J.; Hofer, A.-K.; Bermejo, R.; et al. Texture-engineered ceramics-Property enhancements through crystallographic tailoring. *J. Mater. Res.* **2017**, *32*, 3219–3241. [CrossRef]
11. Haugen, A.B.; Morozov, M.I.; Jones, J.L.; Einarsrud, M.-A. Rayleigh analysis of dielectric properties in textured $K_{0.5}Na_{0.5}NbO_3$ ceramics. *J. Appl. Phys.* **2014**, *116*, 214101. [CrossRef]
12. Grivel, J.C.; Thydén, K.; Bowen, J.R.; Haugen, A.B. Deposition of highly oriented (K,Na)NbO_3 films on flexible metal substrates. *Thin Solid Films* **2018**, *650*, 7–10. [CrossRef]
13. Malič, B.; Koruza, J.; Hrešćak, J.; Bernard, J.; Wang, K.; Fisher, J.G.; Benčan, A. Sintering of lead-free piezoelectric sodium potassium niobate ceramics. *Materials* **2015**, *8*, 8117–8146. [CrossRef] [PubMed]
14. Malič, B.; Benčan, A.; Rojac, T.; Kosec, M. Lead-free piezoelectrics based on alkaline niobates: Synthesis, sintering and microstructure. *Acta Chim. Slov.* **2008**, *55*, 719–726.
15. Li, J.-F.; Wang, K.; Zhu, F.-Y.; Cheng, L.-Q.; Yao, F.-Z. (K,Na)NbO_3-Based Lead-Free Piezoceramics: Fundamental Aspects, Processing Technologies, and Remaining Challenges. *J. Am. Ceram. Soc.* **2013**, *96*, 3677–3696. [CrossRef]
16. Jaffe, B.; Cook, W.; Jaffe, H. *Piezoelectric Ceramics*; Academic Press: Cambridge, MA, USA, 1971.
17. Wang, K.; Li, J.F. (K, Na)NbO_3-based lead-free piezoceramics: Phase transition, sintering and property enhancement. *J. Adv. Ceram.* **2012**, *1*, 24–37. [CrossRef]
18. Fisher, J.G.; Kang, S.J.L. Microstructural changes in $(K_{0.5}Na_{0.5})NbO_3$ ceramics sintered in various atmospheres. *J. Eur. Ceram. Soc.* **2009**, *29*, 2581–2588. [CrossRef]
19. Fisher, J.G.; Rout, D.; Moon, K.S.; Kang, S.J.L. Structural changes in potassium sodium niobate ceramics sintered in different atmospheres. *J. Alloys Compd.* **2009**, *479*, 467–472. [CrossRef]
20. Cen, Z.; Zhen, Y.; Feng, W.; Zhao, P.; Chen, L.; Zhu, C.; Wang, X.; Li, L. Improving piezoelectric properties and temperature stability for KNN-based ceramics sintered in a reducing atmosphere. *J. Am. Ceram. Soc.* **2018**, *101*, 4108–4117. [CrossRef]
21. Zhen, Y.; Cen, Z.; Chen, L.; Zhao, P.; Wang, X.; Li, L. The effect of microstructure on piezoelectric properties and temperature stability for MnO doped KNN-based ceramics sintered in different atmospheres. *J. Alloys Compd.* **2018**, *752*, 206–212. [CrossRef]
22. Kobayashi, K.; Doshida, Y.; Mizuno, Y.; Randall, C.A. A route forwards to narrow the performance gap between PZT and lead-free piezoelectric ceramic with low oxygen partial pressure processed $(Na_{0.5}K_{0.5})NbO_3$. *J. Am. Ceram. Soc.* **2012**, *95*, 2928–2933. [CrossRef]
23. Kawada, S.; Kimura, M.; Higuchi, Y.; Takagi, H. (K,Na)NbO_3-Based Multilayer Piezoelectric Ceramics with Nickel Inner Electrodes. *Appl. Phys. Express* **2009**, *2*, 111401. [CrossRef]
24. Ghosh, D.; Sakata, A.; Carter, J.; Thomas, P.A.; Han, H.; Nino, J.C.; Jones, J.L. Domain wall displacement is the origin of superior permittivity and piezoelectricity in BaTiO3 at intermediate grain sizes. *Adv. Funct. Mater.* **2014**, *24*, 885–896. [CrossRef]
25. Simons, H.; Haugen, A.B.; Jakobsen, A.C.; Schmidt, S.; Stöhr, F.; Majkut, M.; Detlefs, C.; Daniels, J.E.; Damjanovic, D.; Poulsen, H.F. Long-range symmetry breaking in embedded ferroelectrics. *Nat. Mater.* **2018**, *17*, 814–819. [CrossRef] [PubMed]

26. Haugen, A.B.; Madaro, F.; Bjørkeng, L.-P.; Grande, T.; Einarsrud, M.-A. Sintering of sub-micron $K_{0.5}Na_{0.5}NbO_3$ powders fabricated by spray pyrolysis. *J. Eur. Ceram. Soc.* **2015**, *35*, 1449–1457. [CrossRef]
27. Liu, C.; Liu, P.; Kobayashi, K.; Randall, C.A. Base metal Co-fired (Na,K)NbO_3 structures with enhanced piezoelectric performance. *J. Electroceram.* **2014**, *32*, 301–306. [CrossRef]
28. Thong, H.; Xu, Z.; Zhao, C.; Lou, L.; Chen, S.; Zuo, S.; Li, J.; Wang, K. Abnormal grain growth in (K, Na)NbO_3-based lead-free piezoceramic powders. *J. Am. Ceram. Soc.* **2019**, *102*, 836–844.
29. Acker, J.; Kungl, H.; Hoffmann, M.J. Influence of alkaline and niobium excess on sintering and microstructure of sodium-potassium niobate $(K_{0.5}Na_{0.5})NbO_3$. *J. Am. Ceram. Soc.* **2010**, *93*, 1270–1281. [CrossRef]
30. Kizaki, Y.; Noguchi, Y.; Miyayama, M. Defect control for low leakage current in $K_{0.5}Na_{0.5}NbO_3$ single crystals. *Appl. Phys. Lett.* **2006**, *89*, 142910. [CrossRef]
31. Matsubara, M.; Yamaguchi, T.; Kikuta, K.; Hirano, S.I. Effect of Li substitution on the piezoelectric properties of potassium sodium niobate ceramics. *Jpn. J. Appl. Phys.* **2005**, *44*, 6136–6142. [CrossRef]
32. Matthias, B.T.; Remeika, J.P. Dielectric Properties of Sodium and Potassium Niobates. *Phys. Rev.* **1951**, *82*, 727–730. [CrossRef]
33. Cen, Z.; Wang, X.; Huan, Y.; Zhen, Y.; Feng, W.; Li, L. Defect engineering on phase structure and temperature stability of KNN-based ceramics sintered in different atmospheres. *J. Am. Ceram. Soc.* **2018**, *101*, 3032–3043. [CrossRef]
34. Chowdhury, A.; Bould, J.; Zhang, Y.; James, C.; Milne, S.J. Nano-powders of $Na_{0.5}K_{0.5}NbO_3$ made by a sol-gel method. *J. Nanopart. Res.* **2010**, *12*, 209–215. [CrossRef]
35. Chowdhury, A.; O'Callaghan, S.; Skidmore, T.A.; James, C.; Milne, S.J. Nanopowders of $Na_{0.5}K_{0.5}$ NbO_3 Prepared by the Pechini Method. *J. Am. Ceram. Soc.* **2009**, *92*, 758–761. [CrossRef]
36. Vendrell, X.; García, J.E.; Rubio-Marcos, F.; Ochoa, D.A.; Mestres, L.; Fernández, J.F. Exploring different sintering atmospheres to reduce nonlinear response of modified KNN piezoceramics. *J. Eur. Ceram. Soc.* **2013**, *33*, 825–831. [CrossRef]
37. Popovič, A.; Bencze, L.; Koruza, J.; Malič, B. Vapour pressure and mixing thermodynamic properties of the $KNbO_3$–$NaNbO_3$ system. *RSC Adv.* **2015**, *5*, 76249–76256. [CrossRef]
38. Guo, Y.; Kakimoto, K.; Ohsato, H. Phase transitional behavior and piezoelectric properties of (Na[sub 0.5]K[sub 0.5])NbO[sub 3]–LiNbO[sub 3] ceramics. *Appl. Phys. Lett.* **2004**, *85*, 4121. [CrossRef]
39. Irle, E.; Blachnik, R.; Gather, B. The phase diagrams of Na_2O and K_2O with Nb_2O_5 and the ternary system Nb_2O_5-Na_2O-Yb_2O_3. *Thermochim. Acta* **1991**, *179*, 157–169. [CrossRef]
40. Jin, L.; Li, F.; Zhang, S. Decoding the fingerprint of ferroelectric loops: Comprehension of the material properties and structures. *J. Am. Ceram. Soc.* **2014**, *97*, 1–27. [CrossRef]
41. Courths, R.; Steiner, P.; Höchst, H.; Hüfner, S. Photoelectron-spectroscopy investigation and electronic properties of $LiNbO_3$ crystal surfaces. *Appl. Phys.* **1980**, *21*, 345–352. [CrossRef]
42. Morozov, M.I.; Hoffmann, M.J.; Benkert, K.; Schuh, C. Influence of the A/B nonstoichiometry, composition modifiers, and preparation methods on properties of Li- and Ta-modified (K,Na)NbO_3 ceramics. *J. Appl. Phys.* **2012**, *112*, 114107. [CrossRef]
43. Zhao, J.-B.; Du, H.-L.; Qu, S.-B.; Zhang, H.-M.; Xu, Z. Effects of A-site non-stoichiometry on the structural and electrical properties of 0.96K 0.5 Na 0.5 NbO_3—0.04$LiSbO_3$ lead-free piezoelectric ceramics. *Chin. Phys. B* **2011**, *20*, 067701. [CrossRef]